

Roller-Assisted Adhesion Imprinting for High-Throughput Manufacturing of Wearable and Stretchable Organic Light-Emitting Devices

Da Yin, Nai-Rong Jiang, Zhi-Yu Chen, Yue-Feng Liu, Yan-Gang Bi, Xu-Lin Zhang, Jing Feng,* and Hong-Bo Sun*

Stretchable organic optoelectronic devices have been developed rapidly in the last few years due to their great potential in wearable electronics. Although high performance is obtained, high-throughput manufacturing of these devices is still a challenge for their commercial application. Here, a roller-assisted adhesion imprinting (RAI) technique is developed to overcome this challenge by rapid production of ordered and large-area wrinkled structures on organic optoelectronic devices to enable their stretchability. Different from the conventional imprinting technology requiring heating or ultraviolet treatment, adhesion force is employed innovatively in the RAI process to form microstructures within the imprinted materials. As a demonstration, a stretchable wrinkled structure with its length of more than 10 cm is rapidly fabricated and larger area is available by continuous imprinting. Stretchable organic light-emitting devices (SOLEDs) are easily manufactured by the RAI process. The SOLEDs can be elongated to 100% strain and keep working with 5% current efficiency variation after 35 000 cycles of stretching with 20% tensile strain. This is the best mechanical stability of SOLEDs reported to date. The development of the high-throughput, large-area, and cost-effective RAI technique provides potential roll-to-roll continuous production of stretchable electronics.

Organic light-emitting devices (OLEDs) have been considered as very promising candidates for stretchable devices because of their outstanding properties, such as high efficiency, high flexibility, color tunability, and high contrast for displays.^[9–14] Recently, significant progresses have been made in stretchable OLEDs (SOLEDs), including OLEDs array connected by stretchable wires,^[6] intrinsically stretchable polymer LEDs,^[15–17] and wrinkles-based SOLEDs,^[1–3,18,19] which have been summarized systematically by Qian and co-workers.^[20] Stretchability, efficiency, and mechanical stability are surely key issues for practical application of the SOLEDs. Among these various stretching strategies, ordered wrinkles-based SOLEDs are able to satisfy these requirements by exhibiting 100% stretchability, high efficiency of 70 cd A⁻¹, and cyclic stretching stability of withstanding 20 000 stretch-release cycles, respectively.^[1,19] However, high-throughput, large-area, and cost-efficient

Stretchable luminescent devices, based on thin films or fibers, have attracted tremendous attention owing to their great potential in various applications, such as wearable devices,^[1–3] soft and intelligent robots,^[4,5] and deformable displays.^[6–8]

manufacturing of the ordered wrinkles-based SOLEDs is still a challenge.

Roller-associated technology is one of the technologies satisfying the demand of high-throughput production, such as roller imprinting of large-area micro/nanostructures^[21–24] and roll-to-roll production of electronic devices,^[25–29] and has been widely explored from laboratory to industrial production. Here, inspired by this technique, we developed an innovative roller-assisted adhesion imprinting (RAI) toward high-throughput and large-area manufacturing of SOLEDs with ordered wrinkles. In the conventional roller imprinting processes, the assistance of heating^[30,31] or UV irradiation^[32] is necessary to produce softening-curing phase transition of the materials and form surface-relief structures by pressing patterns onto the surface of the target film. Different from those processes, the RAI technology reported here employs adhesion force instead of heating or UV irradiation to change the materials. Large-area periodic wrinkling structure can be directly formed by partly bonding the target film with a supporting substrate. Ordered wrinkles-based SOLEDs have been easily obtained by using flexible and ultrathin OLEDs as the target films. The RAI process

Dr. D. Yin, N.-R. Jiang, Z.-Y. Chen, Dr. Y.-F. Liu, Dr. Y.-G. Bi, Dr. X.-L. Zhang, Prof. J. Feng
State Key Laboratory of Integrated Optoelectronics
College of Electronic Science and Engineering
Jilin University
2699 Qianjin Street, Changchun 130012, China
E-mail: jingfeng@jlu.edu.cn

Prof. H.-B. Sun
State Key Laboratory of Precision Measurement Technology and Instruments
Department of Precision Instrument
Tsinghua University
Haidian, Beijing 100084, China
E-mail: hbsun@tsinghua.edu.cn

 The ORCID identification number(s) for the author(s) of this article can be found under <https://doi.org/10.1002/adom.201901525>.

DOI: 10.1002/adom.201901525

has no negative influence on the performance of the SOLEDs by avoiding the softening-curing phase transition in ultrathin OLEDs. More importantly, the RAI process is beneficial to the mechanical stability of the SOLEDs by effectively maintaining the ordered wrinkles during cyclic stretching through the strong adhesion force between the target film and the elastomeric substrate. As a result, the SOLEDs show comparable efficiency to conventional planar devices and nearly no efficiency variation is observed between 0% and 100% tensile strain. They can keep working during 35 000 cycles of 20% stretching with only 5% current efficiency variation. To the best of our knowledge, this is the best mechanical stability of SOLEDs reported to date.^[1,3,6,12,15–19] The RAI technique is applicable to other stretchable organic electronic and optoelectronic devices and exhibits great potential toward the high-throughput production of the stretchable electronics.

The RAI technology is based on the concept of controllable and selective bonding between the target film and the supporting substrate by adhesion force as illustrated in **Figure 1**. A polymer film as the target film is imprinted onto the prestretched supporting substrate by a patterned roller (Figure 1a and Figure S1, Supporting Information), and they are only allowed to adhere together where the target film is pressed by the roller (Figure 1b). A 50 nm Ag film is first coated on the sticky surface of the supporting substrate as a spacer layer before the imprinting (Figure 1c). The Ag film cracks into

separated and small fragments when the supporting substrate is stretched to 200% strain (Figures 1d and 2a). The width of most fragments and cracks is about tens of microns. The cracked Ag film is proved to be qualified for changing the surface viscosity distribution of the supporting substrate. The supporting substrate loses viscosity where it is covered by Ag film and its sticky surface is exposed again at the cracked regions at stretched states. Only the parts of the target film which are pressed by the roller lines adhere to the exposed sticky surface, while at the pressure-free regions, adhesion is blocked by the Ag fragments as shown in Figure 1e. The pressure-free parts of the target film bend upward after releasing the stretched supporting substrate (Figure 1f). Finally, periodic wrinkles are formed uniformly across the entire target film as shown in **Figure 2c**.

The usage of the Ag spacer layer to change the viscosity of the supporting film is important for ordered wrinkles formation. The supporting substrate is sticky across the whole surface. Without the spacer layer, the uniform viscosity makes the target film and the supporting substrate easily bond together as soon as they get in touch with each other, which results in uncontrollable wrinkles after releasing the prestretched supporting substrate as shown in Figure S2 in the Supporting Information. The thickness of the Ag spacer layer has influence on the shape of the wrinkles. The width of the Ag fragments is increased with their thickness increase as shown in

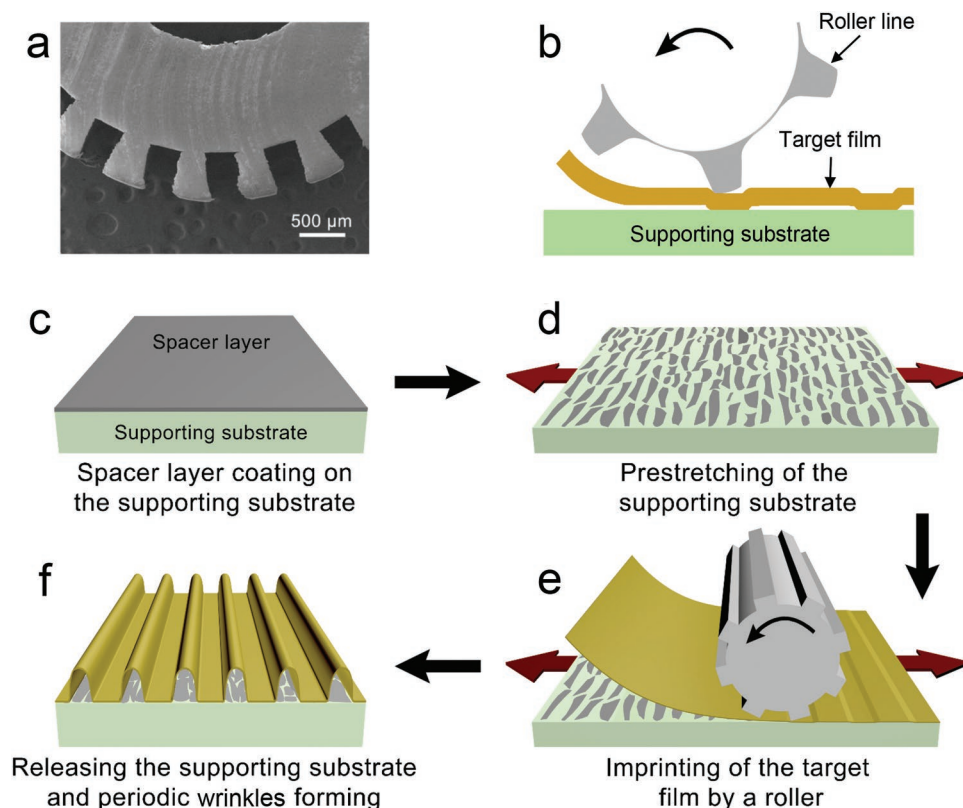


Figure 1. Schematic diagram of the RAI technique. a) SEM image of the patterned roller. b) Concept of selective adhesion between the target film and the supporting substrate controlled by the patterned roller. c) A metallic film coated on the supporting substrate as a spacer layer. d) Prestretching the supporting substrate and the spacer layer cracking to small fragments. e) Imprinting the target film on the prestretched supporting substrate. f) Periodic wrinkles forming after releasing the prestretched supporting substrate.

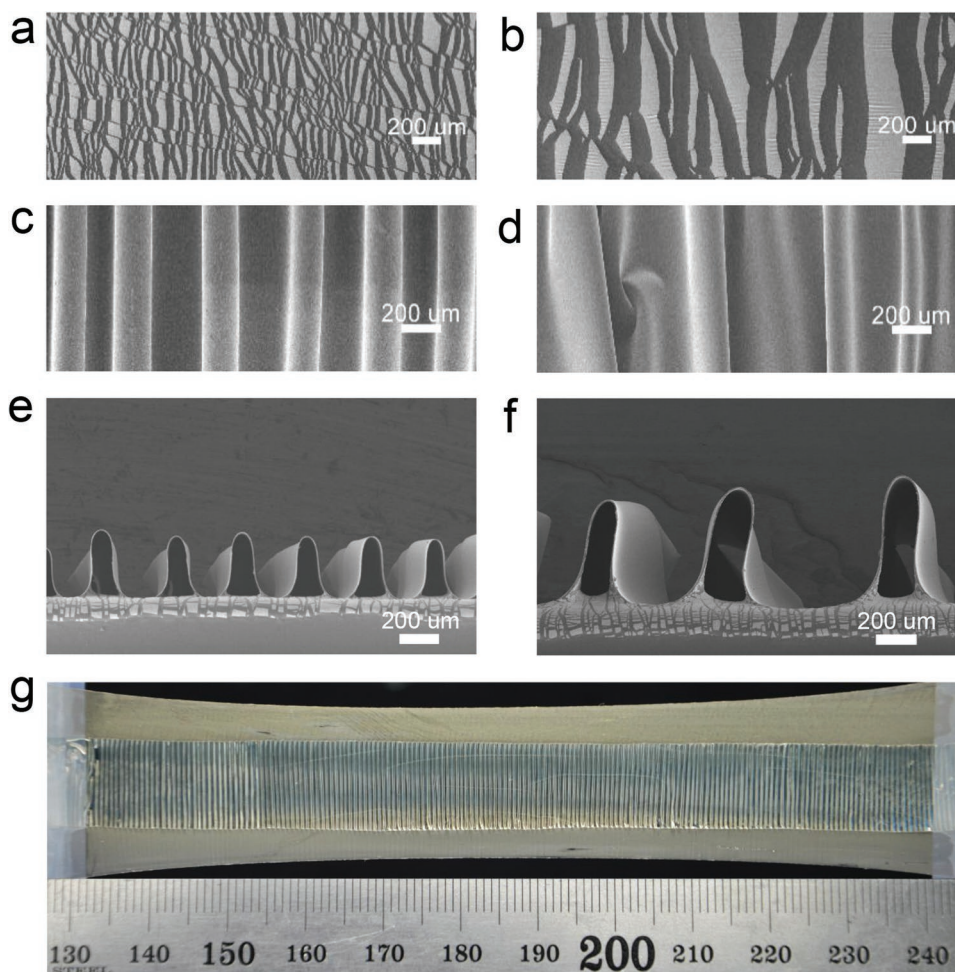


Figure 2. The impact of the thickness of the target film and the spacer layer on the formation of wrinkles. SEM images of the cracked metal spacer layer with thickness of a) 50 nm and b) 100 nm on the supporting substrate with 200% strain, respectively. c) Periodic wrinkles formed by a 2.8 μm thick target film and 50 nm thick Ag spacer layer. d) Disordered wrinkles formed by a 2.8 μm thick target film and 100 nm thick Ag spacer layer. e) Periodic wrinkles formed by a 4.5 μm thick target film and 50 nm thick Ag spacer layer. f) Disordered and larger wrinkles formed by a 6.8 μm thick target film and 50 nm thick Ag spacer layer. g) The photograph of a large-area periodic network of wrinkles. The length unit of the ruler is centimeter.

Figure 2a,b, which would influence the modification effect of the spacer layer on the surface viscosity of the supporting substrate. Ordered wrinkles are formed when the thickness of the Ag film is 50 nm (Figure 2c). When its thickness decreases to less than 20 nm, the modification on the surface viscosity is not enough, which results in the formation of disordered wrinkles (Figure S3, Supporting Information). On the other hand, disordered wrinkles are also formed when its thickness increases to more than 100 nm. This is due to the increased width of the Ag fragments, and some of the fragments are even wider than 200 μm and close to the width of roller lines. In this case, it is possible that some roller lines just roll over the large Ag fragments during the RAI process and the target film are not able to adhere to the supporting substrate, which results in the formation of disordered wrinkles (Figure 2d). Therefore, the width of the Ag fragments should be much smaller than that of the roller lines to form ordered wrinkles.

The thickness of the target film also has impact on the wrinkles formation and is examined by varying its values from 2.8 to 6.8 μm. The thickness of the spacer layer is fixed at 50 nm.

Ordered wrinkles form with the same period for the 4.5 μm target film as shown in Figure 2e. When a 6.8 μm target film is used, the formed wrinkles are larger and not uniform as shown in Figure 2f. This means that the wrinkles formation process is not controllable in this case. The uncontrollability is more obvious when the thickness of the target film further increases to 8.5 μm as shown in Figure S4 in the Supporting Information. It can be attributed to the increased bending strain for the thicker target films, which results in their decreased flexibility. 3D surface morphology of the stretched supporting substrate is measured by laser scanning confocal microscope (Figure S5, Supporting Information). The depth of the cracks among Ag fragments is about 1–2 μm, although the Ag spacer layer is as thin as 50 nm. Local bending deformations must have been produced both in the target film and the supporting substrate to make them contact and bond together during the rolling process. The bending strain (ϵ) of the target film can be approximately expressed as

$$\epsilon = \frac{T}{2R} \quad (1)$$

where T is the film thickness and R is the film bending radius. The thinner 2.8 μm target film has smaller bending strain and is easily deformed and controlled by the roller to form ordered wrinkles. While the bending strain increases about two times in the thicker 8.5 μm target film at the same bending radius. The larger bending strain means that larger pressure is needed to deform the thicker target film. Excessive or insufficient adhesion between the target film and the supporting substrate is liable to happen if the pressure is not uniform during the imprinting process, which makes disordered wrinkles form. According to the above analysis, it can be concluded that a thinner target film will be more suitable for periodic wrinkles formation. As a demonstration, a large-area wrinkling structure with a period of about 650 μm and a length of more than 10 cm has been achieved successfully, in which the Ag spacer layer is 50 nm and an ultrathin polyethylene (PE) sheet ($\approx 3 \mu\text{m}$) is used as the target film (Figure 2g). There are nearly no defects observed in the structure. Larger-scale wrinkling structures are expectable by using larger roller and polymer films. On the other hand, continuous production of ordered wrinkles may

be realized by combining the RAI process with roll-to-roll technique in the future.

SOLEDs based on the periodic wrinkles can be easily obtained by the RAI technique. An ultrathin and flexible OLED with a total thickness of about 3 μm is used as the target film. Phosphorescent material of *tris*(2-phenylpyridine)iridium(III) with green emission is selected to form the emitting layer. The thickness of the Ag spacer layer is 50 nm and the supporting substrate is prestretched to 200% strain. The resulted SOLED with periodic wrinkles is shown in Figure 3a. The wrinkles have a period of about 400 μm at 0% tensile strain. They fade away at the largest 100% tensile strain when re-stretching the supporting substrate (Figure 3b). Figure 3c and Movie S1 in the Supporting Information show the SOLED at working states. Periodic wrinkles have been formed across the entire devices. The stretchability of the SOLED can be improved to 112% by using a roller with larger period in the RAI process (Figure S6, Supporting Information). The strain is concentrated mainly on the regions where wrinkles rise up.^[1] So larger wrinkles are helpful for improving stretchability.

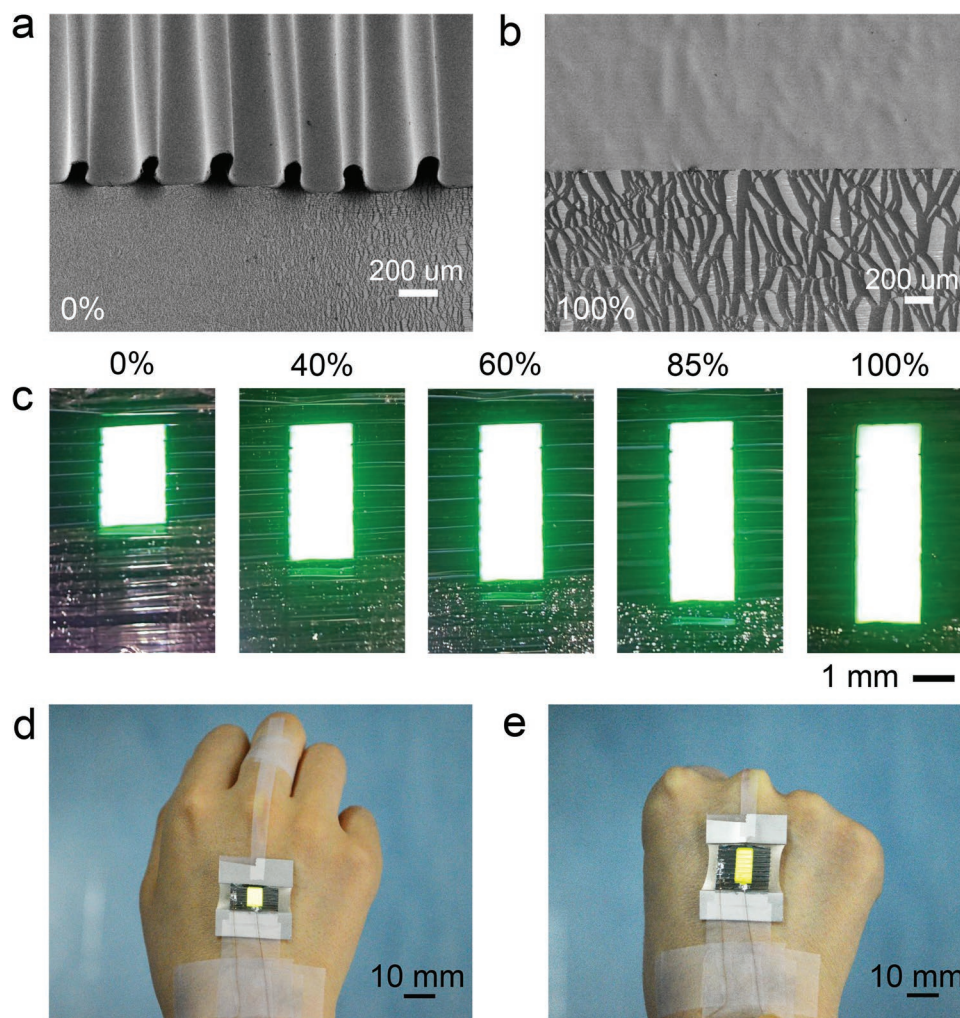


Figure 3. Stretchability of the SOLEDs. SEM images of the SOLEDs at a) 0% strain and at b) 100% strain. c) Photographs of the SOLEDs at strain values increasing from 0% to 100%. d,e) SOLEDs worn on the back of a hand for wearable applications.

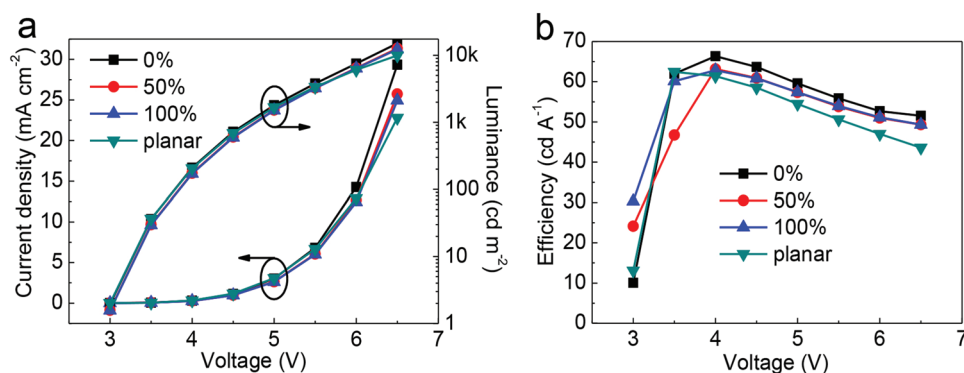


Figure 4. Electroluminescent characteristics of the SOLEDs. a) Luminance and current density characteristics curves and b) efficiency curves of the SOLED and a planar device on Si substrate.

Electronic devices with large stretchability are compatible with deformation of human body and exhibit potential for wearable applications. Here, we bond the SOLED on the back of a hand for wearable applications as shown in Figure 3d,e. A large-area orange phosphorescent OLED is used as the light-emitting unit. It is elongated about 70% when the hand makes a fist. The wrinkles keep ordered during several hand bending cycles as shown in Movie S2 in the Supporting Information. However, it should be noted that the SOLED demonstrated here is not breathable because the device is fabricated on an intact film which prevents gas transmission. Long-time wearing may make skin uncomfortable. Highly breathable SOLEDs for wearable applications are necessary and will be researched in our following work.

The electroluminescence (EL) performance of the green SOLED under different stretching states has been measured. Its EL spectra change with the increasing strain as shown in Figure S7 in the Supporting Information. Narrowing and red-shift occur during the stretching process, which is attributed to the micro-cavity effect.^[18] Figure 4 shows the luminance, current density, and efficiency characteristics of the SOLED. The device at different stretching states exhibits comparable EL performance to a conventional planar device on Si substrate. Combined with the uniform emission of the SOLED (Figure 3c), we can conclude that there is no damage to the device during the imprinting process even though the roller lines contact directly with the device. The bending radii of the wrinkles are between 50 and 100 μm . The OLEDs in a state of tension are still working efficiently, which can be attributed to their small bending strain.^[18,33] The largest luminance of the SOLED is 15 110 cd m^{-2} and its current efficiency reaches 66 cd A^{-1} .

The performance of the SOLEDs under cyclic stretching has been investigated to examine their mechanical stability. The SOLED could survive 35 000 cycles of 20% stretching with only small performance variations (Figure 5a). The luminance degrades 27%, while the efficiency increases 5% which is attributed to the faster decreased current density (Figure S8, Supporting Information). Cyclic stretching at large-range tensile strain of stretchable electronics is required in some cases such as wearable applications.^[1,34,35] Here, cyclic stretching test with 60% strain is examined (Figure 5b). The EL performance of our stretchable device is fairly stable. The current density degrades

about 19% (Figure S9, Supporting Information) while the variations of the luminance and efficiency are only 10% and 11% after 3000 stretch–release cycles, respectively.

Table S1 in the Supporting Information compares the stretching strategy, device type, device processing, maximum stretchability, luminance, efficiency, and cyclic stretching properties of stretchable OLEDs in this work with other published papers. It can be seen that the EL performance and the cyclic stretching stability of the SOLEDs are affected by the stretching strategy obviously. SOLEDs based on ordered wrinkles show higher luminance, current efficiency, and better cyclic stretching stability. Notably, our devices can withstand 35 000 stretch–release cycles with 20% strain, which is the best mechanical stability of SOLEDs among all the results. The excellent mechanical stability is mainly attributed to the RAI-induced stable periodic wrinkling structure, which insures the bending strain of each layer in the OLEDs less than their damage thresholds during the repeated stretch–release cycles. The RAI process induces a strong adhesion force between the ultrathin OLEDs and the supporting substrate, so that no obvious distortion of the wrinkles has been observed after the 35 000 stretch–release cycles, as seen in Figure 5c. This is demonstrated by overstretching the SOLEDs with a strain value larger than 100% as shown in Figure S10 in the Supporting Information. The periodic wrinkles could recover successfully after releasing the strain even though they have been overstretched to crack. No debonding between the ultrathin OLED and the supporting substrate is observed during the overstretching process.

We have developed an RAI technology for ordered wrinkles-based SOLEDs. Adhesion force instead of heating or UV irradiation is employed in this imprinting process to realize the ordered wrinkling structure of the SOLEDs. High throughput and large area can be rapidly obtained benefiting from the continuous fabrication of roller imprinting. The SOLEDs have exhibited excellent performance, especially the recorded mechanical stability with 35 000 cycles of 20% stretching due to the stable structure of the ordered wrinkles induced by the adhesion force. The RAI process shows obvious superiority to the previous methods in commercial applications due to its potential in simple, low-cost, and high-throughput fabrication of the SOLEDs and universal applicability in other stretchable electronics.

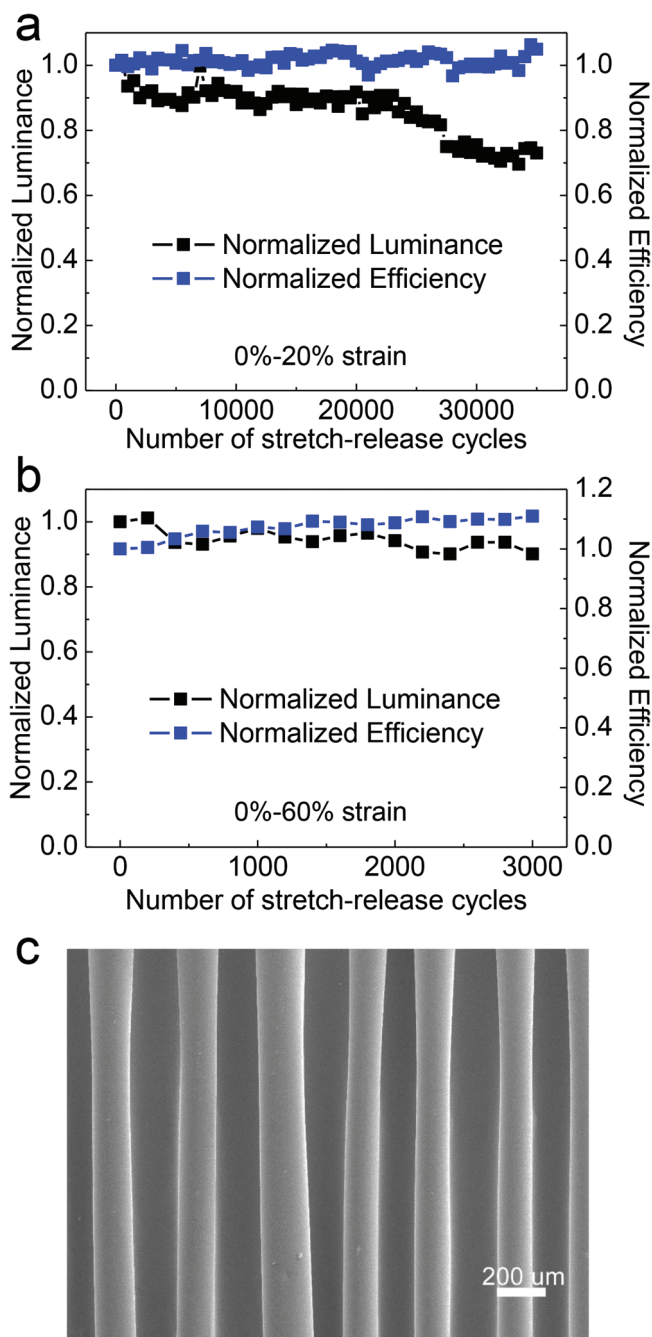


Figure 5. Cyclic stretching test of the SOLEDs. EL performance of the SOLED under cyclic stretching with a) 20% strain and b) 60% strain. c) SEM image of the SOLED after 35 000 cycles of 20% stretching.

Experimental Section

Periodic Wrinkles Fabrication: A series of polymer films (NOA63 photoresist, Norland Products, Inc.) with different thickness was fabricated by spin coating and UV curing process. The spin-coating speed was 12 000, 9000, 7000, and 5000 rpm, respectively. The spin-coating time was 60 s. Ag films with thickness of 20, 50, and 100 nm were coated on the VHB 4905 (3M Company) films as the spacer layers, respectively. The VHB substrates were stretched to 200% strain and the polymer films were attached to the stretched VHB substrates by a lab-made plastic roller. The roller was held by hand via a handle connected

with an axle. The downward pressure on the target polymer films from the roller lines was about 5 N and had small differences during each imprinting process.

For the disordered wrinkles fabricated without the spacer layer, the 2.8 μm thick NOA 63 film was used as the target film.

For the large-area periodic wrinkles fabrication, a transparent and ultrathin PE film was used as the target film. Its thickness was about 3 μm. The PE film was cut into desired size and coated with 30 nm Ag film by thermal evaporation. The metallic film made it easier to observe the wrinkles of the transparent PE film after the imprinting process.

SOLED Fabrication: The ultrathin OLED was prepared by a process as described in the previous work.^[18] The device was fabricated by thermally evaporating the materials of Ag (80 nm), MoO₃ (3 nm), N,N'-diphenyl-N,N'-bis(1,1'-biphenyl)-4,4'-diamine (NPB, 40 nm), N,N'-dicarbazolyl-3,5-benzene (mCP) doped by tris(2-phenylpyridine)iridium(III) (Ir(ppy)₃) (20 nm, 6%), 1,3,5-tris(N-phenyl-benzimidazol-2-yl)benzene (TPBi, 35 nm), and Ca (3 nm)/Ag (18 nm) in sequence. A 50 nm Ag film was thermally coated on the VHB substrate. Then the VHB substrate was stretched to 200% prestrain and the ultrathin OLED was attached to the elastomeric substrate by the RAI process. The experimental parameters during the imprinting process were nearly the same with those described above.

For the SOLED worn on the hand, the orange phosphorescent OLED was fabricated by thermally evaporating Ag (80 nm), MoO₃ (3 nm), NPB (40 nm), 4,4'-bis(N-carbazolyl)-1,1'-biphenyl (CBP) doped by 2,3,5,6-tetrakis(3,6-diphenylcarbazol-9-yl)-1,4-dicyanobenzene (Ir(BT)₂(acac)) (30 nm, 6%), 1,3,5-tris(N-phenyl-benzimidazol-2-yl)benzene (TPBi, 30 nm), and Ca (3 nm)/Ag (18 nm) in sequence. The roller used and the device pictures are shown in Figure S6 in the Supporting Information. The experiments involving human subjects have been performed with the full, informed consent of the volunteers.

Characterizations of the SOLEDs: A home-made moving stage was used to control the stretch–release process. A digital camera was used to take photographs and videos. The scanning electron microscope (SEM) was JEOL JSM-7500F (JOEL Ltd.). The laser scanning confocal microscope was OLYMPUS 3D measuring laser microscope OLS4100. The current of all devices was measured by a Keithley2400 digital sourcemeter and their luminance was measured by a PR 655 in air without encapsulation.

Supporting Information

Supporting Information is available from the Wiley Online Library or from the author.

Acknowledgements

This work was supported by National Natural Science Foundation of China (NSFC) under Grants #61805096, #61825402, #61675085, #61590930 and #61605056.

Conflict of Interest

The authors declare no conflict of interest.

Keywords

ordered wrinkles, roller-assisted adhesion imprinting, stretchable organic light-emitting devices, wearable electronic devices

Received: September 9, 2019

Revised: October 31, 2019

Published online:

- [1] D. Yin, J. Feng, R. Ma, Y. F. Liu, Y. L. Zhang, X. L. Zhang, Y. G. Bi, Q. D. Chen, H. B. Sun, *Nat. Commun.* **2016**, *7*, 11573.
- [2] M. K. Choi, J. Yang, K. Kang, D. C. Kim, C. Choi, C. Park, S. J. Kim, S. I. Chae, T. H. Kim, J. H. Kim, T. Hyeon, D. H. Kim, *Nat. Commun.* **2015**, *6*, 7149.
- [3] T. Yokota, P. Zalar, M. Kaltenbrunner, H. Jinno, N. Matsuhisa, H. Kitanosako, Y. Tachibana, W. Yukita, M. Koizumi, T. Someya, *Sci. Adv.* **2016**, *2*, e1501856.
- [4] C. Larson, B. Peele, S. Li, S. Robinson, M. Totaro, L. Beccai, B. Mazzolai, R. Shepherd, *Science* **2016**, *351*, 1071.
- [5] R.-H. Kim, D. H. Kim, J. Xiao, B. H. Kim, S. I. Park, B. Panilaitis, R. Ghaffari, J. Yao, M. Li, Z. Liu, V. Malyarchuk, D. G. Kim, A. P. Le, R. G. Nuzzo, D. L. Kaplan, F. G. Omenetto, Y. G. Huang, Z. Kang, J. A. Rogers, *Nat. Mater.* **2010**, *9*, 929.
- [6] T. Sekitani, H. Nakajima, H. Maeda, T. Fukushima, T. Aida, K. Hata, T. Someya, *Nat. Mater.* **2009**, *8*, 494.
- [7] S. I. Park, Y. Xiong, R. H. Kim, P. Elvikis, M. Meitl, D. H. Kim, J. Wu, J. Yoon, C. J. Yu, Z. Liu, Y. Huang, K. C. Hwang, P. Ferreira, X. Li, K. Choquette, J. A. Rogers, *Science* **2009**, *325*, 977.
- [8] Z. Zhang, L. Cui, X. Shi, X. Tian, D. Wang, C. Gu, E. Chen, X. Cheng, Y. Xu, Y. Hu, J. Zhang, L. Zhou, H. H. Fong, P. Ma, G. Jiang, X. Sun, B. Zhang, H. Peng, *Adv. Mater.* **2018**, *30*, 1800323.
- [9] J. Feng, Y. F. Liu, Y. G. Bi, H. B. Sun, *Laser Photonics Rev.* **2017**, *11*, 1600145.
- [10] R. Ding, X. P. Wang, J. Feng, X. B. Li, F. X. Dong, W. Q. Tian, J. R. Du, H. H. Fang, H. Y. Wang, T. Yamao, S. Hotta, H. B. Sun, *Adv. Mater.* **2018**, *30*, 1801078.
- [11] H.-W. Chen, J.-H. Lee, B.-Y. Lin, S. Chen, S.-T. Wu, *Light: Sci. Appl.* **2018**, *7*, 17168.
- [12] M. S. White, M. Kaltenbrunner, E. D. Głowacki, K. Gutnichenko, G. Kettlgruber, I. Graz, S. Aazou, C. Ulbricht, D. A. M. Egbe, M. C. Miron, Z. Major, M. C. Scharber, T. Sekitani, T. Someya, S. Bauer, N. S. Sariciftci, *Nat. Photonics* **2013**, *7*, 811.
- [13] T. H. Han, Y. Lee, M. R. Choi, S. H. Woo, S. H. Bae, B. H. Hong, J. H. Ahn, T. W. Lee, *Nat. Photonics* **2012**, *6*, 105.
- [14] J. Xu, Y. Cui, G. M. Smith, P. Li, C. Dun, L. Shao, Y. Guo, H. Wang, Y. Chen, D. L. Carroll, *Light: Sci. Appl.* **2018**, *7*, 46.
- [15] Z. Yu, X. Niu, Z. Liu, Q. Pei, *Adv. Mater.* **2011**, *23*, 3989.
- [16] J. Liang, L. Li, X. Niu, Z. Yu, Q. Pei, *Nat. Photonics* **2013**, *7*, 817.
- [17] J. Liang, L. Li, K. Tong, Z. Ren, W. Hu, X. Niu, Y. Chen, Q. Pei, *ACS Nano* **2014**, *8*, 1590.
- [18] D. Yin, J. Feng, N. Jiang, R. Ma, Y. Liu, H. B. Sun, *ACS Appl. Mater. Interfaces* **2016**, *8*, 31166.
- [19] D. Yin, N. R. Jiang, Y. F. Liu, X. L. Zhang, A. W. Li, J. Feng, H. B. Sun, *Light: Sci. Appl.* **2018**, *7*, 35.
- [20] Y. Qian, X. Zhang, L. Xie, D. Qi, B. K. Chandran, X. Chen, W. Huang, *Adv. Mater.* **2016**, *28*, 9243.
- [21] P. Yi, H. Wu, C. Zhang, L. Peng, X. Lai, *J. Vac. Sci. Technol., B: Microelectron. Nanometer Struct.* **2015**, *33*, 060801.
- [22] H. Tan, A. Gilbertson, S. Y. Chou, *J. Vac. Sci. Technol., B: Microelectron. Nanometer Struct.* **1998**, *16*, 3926.
- [23] J. J. Dumond, Y. L. Hong, *J. Vac. Sci. Technol., B: Microelectron. Nanometer Struct.* **2012**, *30*, 010801.
- [24] N. Kooy, K. Mohamed, L. T. Pin, O. S. Guan, *Nanoscale Res. Lett.* **2014**, *9*, 320.
- [25] S. H. Park, S. J. Lee, J. H. Lee, J. Kal, J. Hahn, H. K. Kim, *Org. Electron.* **2016**, *30*, 112.
- [26] Z. Gao, C. Bumgardner, N. Song, Y. Zhang, J. Li, X. Li, *Nat. Commun.* **2016**, *7*, 11586.
- [27] G. Iannaccone, M. Välimäki, E. Jansson, A. Sunnari, G. Corso, A. Bernardi, M. Levi, S. Turri, J. Hast, G. Griffin, *Sol. Energy Mater. Sol. Cells* **2015**, *143*, 227.
- [28] X. Hu, L. Chen, T. Ji, Y. Zhang, A. Hu, F. Wu, G. Li, Y. Chen, *Adv. Mater. Interfaces* **2015**, *2*, 1500445.
- [29] S. Bae, H. Kim, Y. Lee, X. Xu, J. Park, Y. Zheng, J. Balakrishnan, T. Lei, H. R. Kim, Y. Il Song, Y.-J. Kim, K. S. Kim, B. Özyilmaz, J.-H. Ahn, B. H. Hong, S. Iijima, *Nat. Nanotechnol.* **2010**, *5*, 574.
- [30] S. Y. Chou, P. R. Krauss, P. J. Renstrom, *Appl. Phys. Lett.* **1995**, *67*, 3114.
- [31] S. Y. Chou, P. R. Krauss, W. Zhang, L. J. Guo, L. Zhuang, *J. Vac. Sci. Technol., B: Microelectron. Nanometer Struct.* **1997**, *15*, 2897.
- [32] J. Haisma, M. Verheijen, K. van den Heuvel, J. van den Berg, *J. Vac. Sci. Technol., B: Microelectron. Nanometer Struct.* **1996**, *14*, 4124.
- [33] Z. Suo, E. Y. Ma, H. Gleskova, S. Wagner, *Appl. Phys. Lett.* **1999**, *74*, 1177.
- [34] T. Yamada, Y. Hayamizu, Y. Yamamoto, Y. Yomogida, A. Izadi-Najafabadi, D. N. Futaba, K. Hata, *Nat. Nanotechnol.* **2011**, *6*, 296.
- [35] S. H. Jeong, S. Zhang, K. Hjort, J. Hilborn, Z. Wu, *Adv. Mater.* **2016**, *28*, 5830.